# Optical second-harmonic generation at total reflection in a potassium dihydrogen phosphate crystal

V. Bhanthumnavin
*Department of Physics and Institute of Science, Suranaree University of Technologies, Suranaree, Ampure Muang, Nakoranrajsima 3000, Thailand*

Chi H. Lee*
*Department of Electrical Engineering, University of Maryland, College Park, Maryland 20742*
(Received 4 October 1993)

The intensity of a second-harmonic light beam generated in potassium dihydrogen phosphate (KDP) crystals immersed in the optically dense fluid 1-bromonaphthalene has been observed as a function of the incident angle of the fundamental beam of a mode-locked neodymium glass laser. The laser pulses have polarization in the [1$\bar{1}$0] direction with respect to the KDP crystallographic axes. The phase-matchable second-harmonic generation at total reflection and in the vicinity of the critical angle were performed. The existence of a nonlinear Brewster angle has been demonstrated and its utilization may include using a null method for a precise measurement of the relative magnitude of nonlinear optical susceptibility components of materials. The results agree well with the theory of Bloembergen and Pershan [Phys. Rev. **128**, 606 (1962)].

PACS number(s): 42.65.Ky

## I. INTRODUCTION

Over the last three decades, there has been a great deal of research done in the area of nonlinear optics. In the domain of second-harmonic generation (SHG), most of the attention has been directed toward SHG in transmission in a phase-matchable condition for maximum conversion efficiency. Extension of the fundamental optical phenomena from the linear to the nonlinear regime will not be completed, however, if the basic nonlinear interaction at the boundary between a linear and nonlinear medium is not fully investigated [1]. This is the area that has not been fully exploited. Only a limited amount of work has been reported, in particular, when the fundamental beam is at total internal reflection [2–7].

In addition to SHG near total reflection, there have been a number of device applications employing nonlinear optical interaction or the electro-optic effect at total internal reflection [8–14]. The electro-optic effect at total internal reflection can be regarded as a nonlinear interaction between the low-frequency microwave and the high-frequency optical wave at the boundary of the nonlinear medium. This theoretical optical model explains experimental data of electro-optical reflectance near the critical angle well. The theoretical formalism for the electro-optic effect is essentially the same as SHG described in this work. Thus it is important to have a good understanding of the nonlinear phenomena taking place at the boundary of the nonlinear medium, in particular, when the fundamental beam is obliquely incident. Recently, obliquely incident beams producing nonlinear optical phenomena have also gained attention because they can be used as a tool to probe solid-solid interfaces [15,16]. This is due to the fact that traditional optical spectroscopies lack interface specificity and most surface diagnostic techniques are inconvenient for studying buried interfaces. Although the work reported here is for a liquid-solid interface, it can easily be extended to study buried solid-solid interfaces.

The reflection of laser light at the interface between linear and nonlinear media at an oblique angle of incidence $\theta_i$ near the critical angle $\theta_{cr}$ can provide interesting nonlinear optical effects as predicted by the Bloembergen-Pershan (BP) theory [1]. In our experiment, the investigation of second-harmonic generation in the vicinity of the critical angle $\theta_{cr}(\omega)$ has been performed at total reflection. This leads to the verification of nonlinear optical effects [3,6,17]. Furthermore, using the same crystallographic cut of potassium dihydrogen phosphate (KDP) [6], the work was extended theoretically for a nonlinear Brewster angle in ammonium dihydrogen phosphate (ADP) [18].

It is the purpose of this paper to present a quantitative study of second-harmonic generation in reflection with oblique incidence of the fundamental beam. The special emphasis is SHG in reflection in the vicinity of critical angles $\theta_{cr}(\omega)$ and $\theta_{cr}(2\omega)$. The "walk-off" effect in phase-matched SHG at total reflection is performed and analyzed. Furthermore, the existence of the nonlinear Brewster angle has been demonstrated and its utilization may include using a null method for the precise measurement of the relative magnitude of nonlinear optical susceptibility components of materials. The experimental results agree well with the prediction of both the BP theory [1] and a theory by Dick *et al.* [19].

In Sec. II, the BP theory is given in a form which will

*FAX: 301-314-9281.

 

permit direct comparison with the experiment using a KDP uniaxial crystal. In Sec. III, the experimental arrangement is described and in Sec. IV the experimental results are given and compared with the theories. Section V is the conclusion from the experimental results.

## II. THEORY

The geometrical situation just before total reflection occurs is shown in Fig. 1. The fundamental beam is transmitted almost parallel to the surface in the nonlinear crystal KDP. According to the theory of Bloembergen and Pershal [1], there are reflected, inhomogeneous, and homogeneous harmonic beams. The driven polarization wave propagates in the same direction as the transmitted fundamental beam. It has a wave vector $\mathbf{k}_s(2\omega)=2\mathbf{k}_L(\omega)$ which represents the particular solution of the inhomogeneous wave equation. In addition there is the homogeneous solution with wave vector $\mathbf{k}_T(2\omega)$. In the nonlinear crystal KDP the two transmitted harmonic beams are spatially distinct and readily observed separately. As the angle of incidence $\theta_i$ in Fig. 1 increases, it is intuitively clear that the beam with wave vector $\mathbf{k}_s$ will disappear at the same time as the transmitted fundamental beam. The transmitted harmonic beam with wave vector $\mathbf{k}_T(2\omega)$ will still persist. Second-harmonic power can be transmitted even when the fundamental power is totally reflected. For large angle of incidence $\theta_i$, this second-harmonic wave eventually also disappears and only the reflected harmonic wave remains.

The geometry of wave vectors of the fundamental $\mathbf{K}^i$ and harmonic light wave $\mathbf{K}^R$, $\mathbf{K}^S$, and $\mathbf{K}^T$ at the boundary between 1-bromonaphthalene and the uniaxial crystal KDP is depicted in Fig. 2. The angles $\theta_R$, $\theta_S$, and $\theta_T$ of the reflected, inhomogeneous, and homogeneous transmitted waves, respectively, are given by the generalized Snell's law

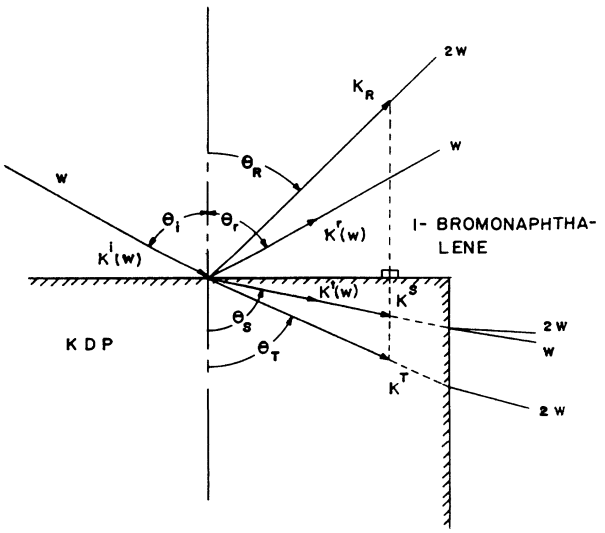


FIG. 1. Behavior of fundamental and second-harmonic waves in the neighborhood of total reflection.

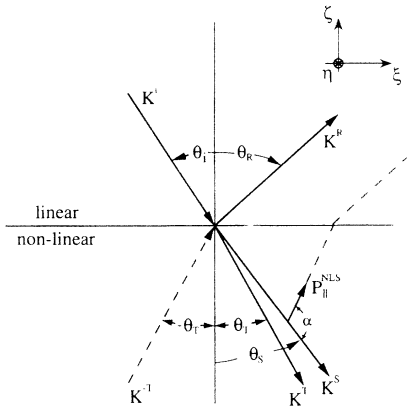


FIG. 2. Physical interpretation of the nonlinear Brewster angle.

$$n_{\text{liq}}(\omega)\sin\theta_i = n_{\text{liq}}(2\omega)\sin\theta_R = n(\omega)\sin\theta_S = n(2\omega)\sin\theta_T \ . \tag{1}$$

The refractive indices without subscripts refer to the KDP crystal.

The components of nonlinear source polarization $\mathbf{P}^{\text{NLS}}(2\omega)$ along the cubic axes of the nonlinear KDP crystal are given in terms of the fundamental field components at each point inside the crystal by

$$P_z^{\text{NLS}}(2\omega)=\chi_{36}^{\text{NL}}E_x^T(\omega)E_y^T(\omega) \ . \tag{2}$$

$P_x^{\text{NLS}}(2\omega)$ and $P_y^{\text{NLS}}(2\omega)$ can be obtained by cyclic permutation of Eq. (2).

The KDP crystal in the experiment has an orientation such that the $z$ (optic) axis which is in the [001] direction lies in the plane of incidence. The incident fundamental field is polarized perpendicular to the plane of incidence and is the $[1\bar{1}0]$ direction with respect to the crystallographic axes of the KDP. $\mathbf{P}^{\text{NLS}}(2\omega)$ will be along the [001] direction and also is in the plane of incidence. $P_z^{\text{NLS}}(2\omega)$ given by Eq. (2) can be expressed in terms of the amplitude $E_0$ of the fundamental wave by

$$P_z^{\text{NLS}}(2\omega)=\chi_{36}^{\text{NL}}\eta(F_T^L E_0)^2 \ , \tag{3}$$

where $\eta$ is a geometrical factor that depends on the orientation of the fundamental field vector and nonlinear polarization component with respect to the crystallographic cubic axes of the KDP. The linear Fresnel factor $F_T^L$ describes the change of amplitude of the fundamental wave upon transmission at the crystal surface. If the laser polarization is perpendicular to the plane of incidence, $F_T^L$ is given by

$$F_T^L=\frac{2\cos\theta_i}{\cos\theta_i+\sin\theta_{\text{cr}}(\omega)\cos\theta_S} \ , \tag{4}$$

where $\theta_{\text{cr}}(\omega)$ is the critical angle of incidence of the fundamental beam.

The nonlinear polarization is the source of the three

harmonic waves. The electric field amplitudes of the reflected harmonic wave are given by

$$E_R(2\omega)=4\pi P^{\mathrm{NLS}}F_R^{\mathrm{NL}} , \tag{5}$$

where $F_R^{\mathrm{NL}}$ is the nonlinear Fresnel factor.

For the case of nonlinear polarization, $\mathbf{P}^{\mathrm{NLS}}(2\omega)$ lying in the plane of incidence, the nonlinear Fresnel factor $F_{R,11}^{\mathrm{NL}}$, according to the BP theory is given by

$$F_{R,11}^{\mathrm{NL}}=\frac{\sin\theta_S\sin^2\theta_T\sin(\alpha+\theta_S+\theta_T)}{\epsilon_R(2\omega)\sin\theta_R\sin(\theta_T+\theta_R)\sin(\theta_T+\theta_S)\cos(\theta_T-\theta_R)} , \tag{6}$$

where $\epsilon^{1/2}(2\omega)=n_{\mathrm{liq}}(2\omega)$. The angle $\alpha$ is the angle between the nonlinear polarization $\mathbf{P}^{\mathrm{NLS}}(2\omega)$ in the plane of incidence and the direction of the source vector $\mathbf{k}_S$, as shown in Fig. 2. It is emphasized that this expression remains valid in the case of total reflection [2,3,17].

The time-averaged second-harmonic power carried by the harmonic beam is given by the product of the real part of the Poynting vector and the cross-sectional area $A$ of the beam.

$$I_R(2\omega)=\left[\frac{c}{8\pi}\right]\epsilon_R^{1/2}(2\omega)|E_R(2\omega)|^2A_R . \tag{7}$$

The $I_R(2\omega)$ in Eq. (7) is the intensity integrated over the beam cross section, or power. This is the experimentally observed quantity. In the remainder of this paper, intensity and power will be used interchangeably in a similar manner [3,6,17]. $A_R$ in Eq. (7) is the cross-sectional area of the beam and is given by

$$A_R=(dd'\cos\theta_R)/\cos\theta_i , \tag{8}$$

where $dd'$ is the area of the rectangular slit which defines the size of the incident laser beam. By substitution of the relevant expression into Eq. (7), we finally obtain

$$I_R(2\omega)=(c/8\pi)\epsilon_R^{1/2}|E_0|^4dd'(4\pi\chi_{36}^{\mathrm{NL}})^2\eta^2 \times|F_T^L|^4|F_R^{\mathrm{NL}}|^2\cos\theta_R(\cos\theta_i)^{-1} \tag{9}$$

for the intensity of the reflected harmonic wave. The expression in (9) facilitates obtaining the theoretical curve of intensity of the reflected harmonic wave for comparison to the experimental data.

A uniaxial KDP crystal is employed for reflected second-harmonic generation (SHG) at the phase-matching condition by birefringence. The phase-matching angle $\theta_m$ is determined by making the birefringence $(n_0^{2\omega}-n_e^{2\omega})$ equal to the dispersion $(n_0^{2\omega}-n_0^{\omega})$ at the phase-matching angle $\theta_m$; and $n_e^{2\omega}=n_0^{\omega}$ at this condition. However, SHG may still be limited by double refraction which is describable by an angle $\rho$ between the Poynting vector of the extraordinary harmonic wave and the ordinary fundamental wave. The angle $\rho$ is given by [20]

$$\tan\rho=\tfrac{1}{2}[n_e^{2\omega}(\theta)]^2\left\{\frac{1}{[n_e^{2\omega}(\pi/2)]^2}-\frac{1}{[n_0^{2\omega}]^2}\right\}\sin2\theta , \tag{10}$$

where $\theta$ is the angle between the propagation vector of the homogeneous second-harmonic beam and the optic axis. Furthermore, determination of $n_e^{2\omega}(\theta)$ for a specific value of $\theta$ can be obtained from the equation of the index ellipsoid, given by

$$\frac{1}{[n_e^{2\omega}(\theta)]^2}=\frac{\cos^2\theta}{[n_0^{2\omega}]^2}+\frac{\sin^2\theta}{[n_e^{2\omega}(\pi/2)]^2} . \tag{11}$$

## III. EXPERIMENTAL TECHNIQUE

### A. KDP crystal preparation

The nonlinear crystal used in the experiment was uniaxial KDP with crystallographic cuts as indicated in Sec. IV. The KDP crystal is transparent at the fundamental and second-harmonic wavelengths. This allows an investigation in transmission. Furthermore, its linear index of refraction is relatively low, and therefore total reflection from it is possible via the optically denser linear fluid 1-bromonaphthalene. Typical dimensions of the KDP crystal used in the experiment were $15\times25\times8$ mm$^3$. The entrance and exit surfaces were polished optically flat to $\lambda/5$ at the $D$ line of sodium light. The parallelism between the two opposite faces was better than 30″ and none of the surfaces were coated. The refractive indices of the KDP crystal at the fundamental and second-harmonic frequencies are

$$n_0^{\omega}=1.4943 , \quad n_0^{2\omega}=1.5130 , \quad n_e^{2\omega}c\pi/2=1.4708 .$$

The crystal was mounted on an aluminum holder which was connected to an angular rotational device mounted on a platform above the liquid cell. The variation of the angle of incidence $\theta_i$ was performed by a rotational device which has the axis of rotation tangential to the incident surface of the crystal. The crystal could be positioned with an accuracy of 0.01°.

### B. Optically denser fluid

The KDP crystal was immersed in the optically denser fluid 1-bromonaphthalene which has larger indices than the crystal at both the frequencies $\omega$ and $2\omega$. The fluid is transparent in the range of wavelengths 0.4–1.6 $\mu$m. The indices of refraction of the fluid at the fundamental and second-harmonic frequencies are

$$n_{\mathrm{liq}}(\omega)=1.6262 \quad \text{and} \quad n_{\mathrm{liq}}(2\omega)=1.6701 ,$$

respectively. From Eq. (1) we found that the critical angles for total reflection are

$$\theta_{\mathrm{cr}}(\omega)=66.78^\circ \quad \text{and} \quad \theta_{\mathrm{cr}}(2\omega)=64.76^\circ .$$

Furthermore, the investigation by using 1-bromonaphthalene which has a larger index of refraction than the KDP crystal will enable us to perform phase-matched second-harmonic generation at total reflection. Under these conditions where $\mathbf{P}^{\mathrm{NLS}}(2\omega)$ in the [001] direction makes a phase-matching angle $\theta_m = 41.2°$ with respect to the surface of the KDP crystal, a nonlinear Brewster angle was observed [6].

### C. Optical arrangement

The laser used in the experiment was a standard $Q$-switched mode-locked Nd:glass laser system with Brewster cuts at both ends of the Nd:glass rod as shown in Fig. 3. The fundamental beam was linearly polarized by means of a Glann-Kappa prism. To ensure that the fundamental beam was polarized along the $[1\bar{1}0]$ direction with respect to the crystallographic axes of KDP, a half-wave plate was used to rotate the electric field of the fundamental beam from horizontal to vertical polarization. The fundamental beam before entering the liquid cell was regulated by a rectangular slit which was $1\times5$ mm$^2$. The liquid cell had a hexagonal shape with six circular fixed quartz windows. The detecting system for SHG from the KDP crystal was mounted on an aluminum arm pivoted underneath the liquid cell. The axis of rotation of the arm was the same as the axis of the crystal rotation, which was the linear tangent to the incident surface of the KDP. The second-harmonic signal was isolated from the fundamental by the standard spectral filtering technique as indicated in Fig. 3. A slit of $4\times10$ mm$^2$ situated at 50 cm away from the liquid cell was used in the detecting arm for separation of the reflected or transmitted second-harmonic intensities from the reflected or transmitted fundamental beam, respectively. Each data point was normalized by the monitor intensity in order to eliminate the effect caused by laser intensity fluctuation and the nonlinear optical process of second-harmonic generation.

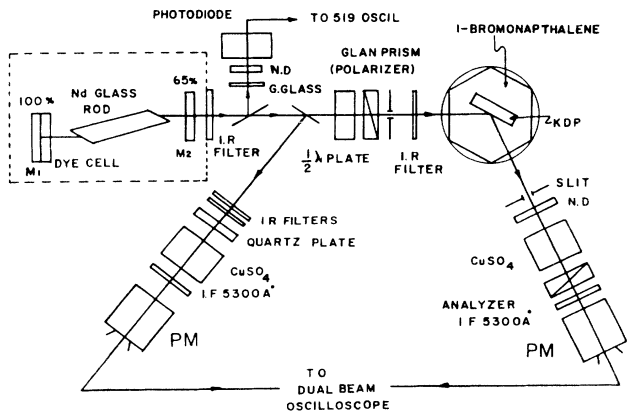


FIG. 3. Experimental arrangement for measuring reflected second-harmonic intensity (SHI). The symbols are defined as follows: PM, photomultiplier; IF, interference filter; IR, infrared; ND, neutral density filter; and G. Glass, ground glass.

## IV. EXPERIMENTAL RESULTS

The experimental results for the intensity of the reflected second-harmonic beam are presented for several cases of KDP with different orientations of $\mathbf{P}^{\mathrm{NLS}}(2\omega)$.

### A. Non-phase-matching second-harmonic generation at total reflection

A KDP crystal of dimensions $25\times15\times8$ mm$^3$, where the entrance surface for the fundamental beam was $25\times15$ mm$^2$, was used in this experiment. The face normal to the entrance surface was along the optic axis which is the [001] direction and parallels $\mathbf{P}^{\mathrm{NLS}}(2\omega)$ as indicated in Fig. 4. The polarization of the fundamental beam was along the $[1\bar{1}0]$ direction with respect to the crystallographic axes of the crystal. The reflected second-harmonic intensity generated from the KDP crystal immersed in 1-bromonaphthalene was observed as a function of the angle of incidence $\theta_i$. The theoretical curve was calculated from the expression

$$|F_T^L|^4 |F_{R,11}^{\mathrm{NL}}|^2 \cos\theta_R (\cos\theta_i)^{-1}$$

of Eq. (9). The result of the experiment is shown in Fig. 4. The solid curve represents the result of the theoretical calculation. The figure shows an excellent agreement between the experimental data and the result predicted by BP theory. There are two cusps at $\theta_{\mathrm{cr}}(\omega)$ and $\theta_{\mathrm{cr}}(2\omega)$, respectively. The theoretical curve reflects the influence of the linear and nonlinear Fresnel factors given by Eqs. (4)

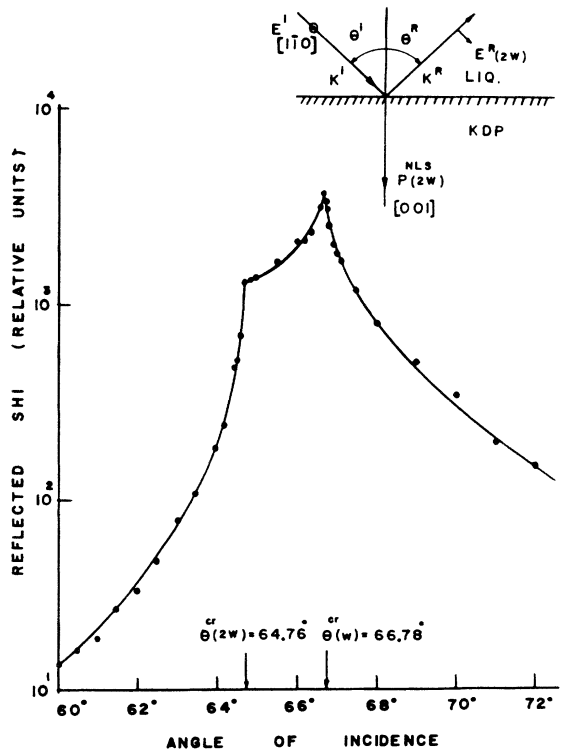


FIG. 4. Reflected second-harmonic intensity (SHI) from a KDP crystal of non-phase-matchable orientation in the neighborhood of the critical angle for total reflection.

and (6) when $\theta_i$ approaches $\theta_{cr}(\omega)$ and $\theta_{cr}(2\omega)$. Nonanalytical singularities occur at $\theta_i=\theta_{cr}(\omega)$ and $\theta_i=\theta_{cr}(2\omega)$, respectively, as expected from BP theory. The reason for the appearance of two cusps at critical angles $\theta_{cr}(\omega)$ and $\theta_{cr}(2\omega)$ is that at these critical angles the value of $\cos\theta_S$ and $\cos\theta_T$ change from real to imaginary values. This experimental feature was not clearly observed in the earlier experiment [3] of this sort. We attribute the success here to the fact that in our experiment a mode-locked laser beam was used, and therefore multimode effects in the nonlinear process are minimized [2].

The enhancement of the reflected second harmonic intensity in the vicinity of the critical angles $\theta_{cr}(\omega)$ and $\theta_{cf}(2\omega)$ arises mainly from two sources. First, the linear Fresnel factor $F^L$ near the critical angle $\theta_{cr}(\omega)$ is larger than it is away from this angle, by a factor of approximately 2. This gives an increase by a factor of 16 in the reflected second-harmonic intensity $I_R(2\omega)$ in Eq. (9). Second, the nonlinear Fresnel factor $F^{NL}_{R,11}$, defined in Eq. (6), is dominated in the vicinity of $\theta_{cr}(\omega)$ and $\theta_{cr}(2\omega)$ by the term $[\sin(\theta_S+\theta_T)]^{-1}$, and it is larger than that away from these points by a factor of 3. Therefore, after all factors are accounted for, the additional enhancement of $I_R(2\omega)$ in the vicinity of the critical angles will be about two orders of magnitude, as indicated in Fig. 4.

It is interesting to consider the limiting case when $\theta_{cr}(\omega)$ and $\theta_{cr}(2\omega)$ coalesce into a single value [7]. Under this condition, the wave vectors $\mathbf{K}_S$ and $\mathbf{K}_T$ will propagate along the same direction, i.e., along the crystal surface, because of total internal reflection. Since the crystal was cut with the phase-matching direction along the crystal surface, the two critical angles $\theta_{cr}(\omega)$ and $\theta_{cr}(2\omega)$ merged into one and the additional enhancement of $I_R(2\omega)$ occurred as a result of phase matching, as indicated in Fig. 5 [7]. One can consider the curve shown in Fig. 5 as a limiting case of that of Fig. 4. When the phase-matching condition at total reflection prevailed, the two cusps in Fig. 4 collapsed into a single maximum peak of $I_R(2\omega)$ at $\theta_{cr}(\omega)$.

### B. "Walk-off" effect in phase-matched second-harmonic generation at total reflection

Phase-matched SHG at total reflection using KDP has been demonstrated [7]. In our case, a KDP crystal with the orientation indicated in Fig. 5 was employed but the $\mathbf{P}^{NLS}(2\omega)$ is now rotated 180° about the crystal face normal. The situation is shown in Fig. 6. It was anticipated that the phase-matched SHG from the KDP crystal which has $\mathbf{P}^{NLS}(2\omega)$ oriented as indicated in Fig. 6 will yield the same result as that of Fig. 5. However, the experimental data shown in Fig. 6 indicate that this is not the case. According to the KDP crystallographic cut the value of $F^{NL}_{R,11}$ in Eq. (6) tends to go to infinity when $\theta_i=\theta_{cr}(\omega)$, which leads to $\theta_S=\theta_T=\pi/2$, where the phase-matching condition prevails. From the experimental result in Fig. 6, the $I_R(2\omega)$ increased by about two orders of magnitude when the angle of incidence approached the critical angle $\theta_{cr}(\omega)$. The maximum of $I_R(2\omega)$ occurred at the critical angle $\theta_{cr}(\omega)$ and in good agreement with the prediction of BP theory. It is found

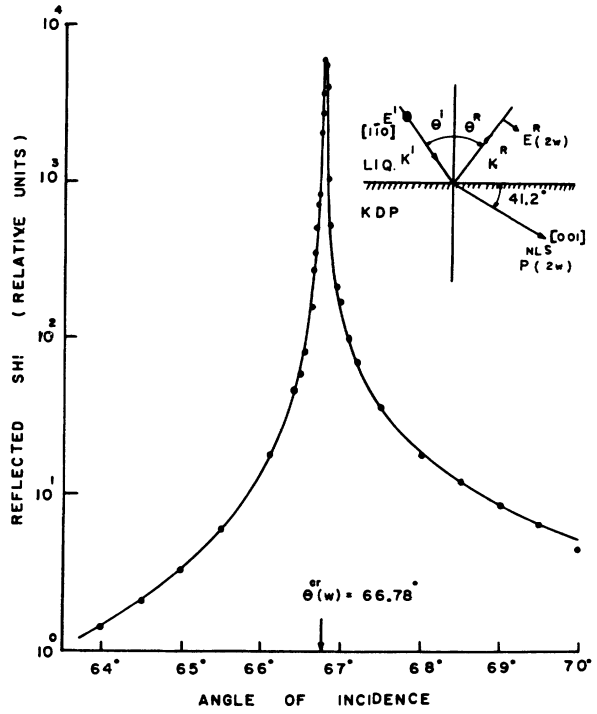


FIG. 5. Reflected second-harmonic intensity (SHI) from a KDP crystal with phase matching at total reflection [7].

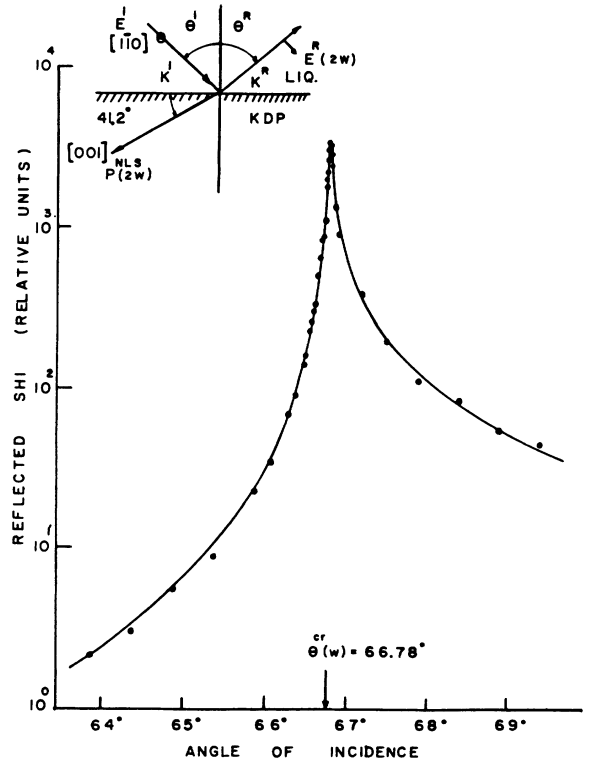


FIG. 6. Reflected second-harmonic intensity (SHI) from a KDP crystal (rotated 180° about the face normal) with phase matching at total reflection.

that the overall shape of $I_R(2\omega)$ in Fig. 6 is broader and in addition the peak intensity is lower than that in Fig. 5 by about one order of magnitude. The difference of $I_R(2\omega)$ in the two cases can be understood by the fact that the KDP crystal is a uniaxial crystal with an angular-dependent extraordinary index of refraction. For second-harmonic generation from a uniaxial crystal there exists a "walk-off" effect, which will reduce the second-harmonic generation inside the crystal [21]. The "walk-off" effect refers to the phenomenon that the second harmonic polarization and radiation waves become spatially separated because of their finite beam size in a uniaxial crystal. Inside the uniaxial crystal, for any given direction of phase-front propagation, the direction of energy propagation (Poynting vector) is along the normal to the normal (index) surface. For the case of an ordinary wave, the propagation $k$ vector and the Poynting vector are parallel. However, for the extraordinary wave the Poynting vector deviates from the phase propagation direction by an angle $\rho$, called the angle of double refraction. Its expression is given by Eq. (10).

The index ellipsoids of both ordinary and extraordinary indices of KDP for the phase-matching conditions corresponding to the orientation of the KDP crystals used in the experiment of Figs. 5 and 6 are depicted in Fig. 7. The fundamental wave takes the index surface of an ordinary ray and the homogeneous second harmonic takes the index surface of an extraordinary ray. In Fig. 7, the drawing indicates the conservation of the tangential components of the $\mathbf{K}$ vectors. The vectors $\mathbf{K}^a$ and $\mathbf{K}^b$ correspond to the geometries of KDP orientation used in Figs. 5 and 6, respectively. At total reflection $\mathbf{K}_S^a=0A$, $\mathbf{K}_S^b=0C$. According to the normal (index) surfaces and boundary conditions of the $\mathbf{K}$ vectors, $\mathbf{K}_T$ may take two values, i.e., $\mathbf{K}_T^a=\mathbf{K}_S^a=0A$ or $\mathbf{K}_T^a=0B$. However, the former situation of $\mathbf{K}_T^a=0A$ would give a ray velocity propagating out of the nonlinear medium, i.e., the energy propagates out of the medium. This is not a physically allowed situation. Thus the only physically allowed situation is that of $\mathbf{K}_T^a=0B$ for the case of KDP in Fig. 5 and $\mathbf{K}_T^b=0C$ for the case of KDP in Fig. 6. The corresponding incident wave vectors are $\mathbf{K}_i^a$ and $\mathbf{K}_i^b$, respectively.

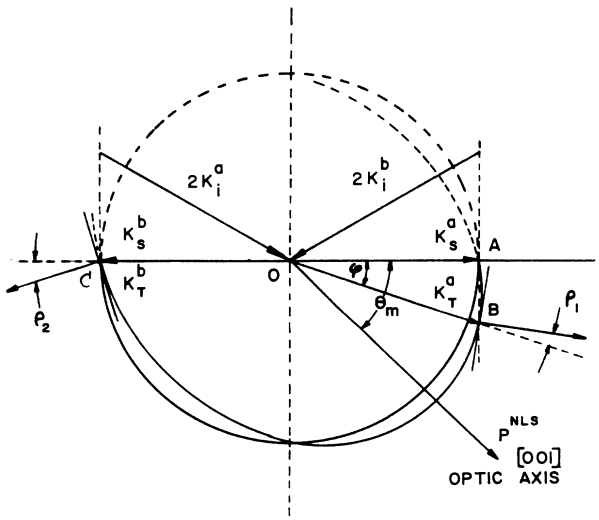


FIG. 7. Geometrical construction to demonstrate the effect of turning a KDP crystal by 180° (about the face normal) on the determination of a physically allowed solution for the $\mathbf{K}$ vectors of harmonic waves in a nonlinear medium.

Furthermore, the angle $\varphi$ in Fig. 7 can be obtained from Eq. (11) and

$$n_e^{2\omega}(41.2°-\varphi)\cos\varphi=n_0^{\omega} . \tag{12}$$

The angle $\varphi$ and consequently $n_e^{2\omega}(41.2°-\varphi)$ are found to be

$$\varphi=1.12° ,$$
$$n_e^{2\omega}(41.2°-1.12°)=n_e^{2\omega}(40.08°)=1.4946 . \tag{13}$$

The values of $\varphi=1.12°$ and $n_e^{2\omega}(40.08°)=1.4946$ correspond to the case of $\mathbf{K}_T^a=0B$.

For the case of $\mathbf{K}_T^b=0C$, the angle $\varphi=0$ and $n_e^{2\omega}(\theta)$ takes the value $n_e^{2\omega}(41.2°)=n_0^{\omega}=1.4943$. By substitution of $n_e^{2\omega}(40.08°)=1.4946$ and $n_e^{2\omega}(41.2°)=1.4943$ into Eq. (10), the angles $\rho_1$ and $\rho_2$ are found to be

$$\rho_1=1.07° \text{ and } \rho_2=1.08° ,$$

respectively. Therefore, the angle between the directions of energy propagation of $\mathbf{K}_S^a$ and $\mathbf{K}_T^a$ corresponding to the orientation of KDP in Fig. 5 is

$$\varphi-\rho_1=1.12°-1.07°=0.05°$$

whereas the angle between the directions of energy propagation of $\mathbf{K}_S^b$ and $\mathbf{K}_T^b$ corresponding to the orientation of KDP in Fig. 6 is $\rho_2=1.08°$. Thus, for the case of KDP in Fig. 5, the polarization and radiation waves will have greater overlap and hence a larger volume of interaction which will lead to more intense reflected second-harmonic intensity $I_R(2\omega)$ with a narrower peak than that of Fig. 6.

### C. Nonlinear Brewster angle

According to BP theory, a nonlinear Brewster angle is predicted for second-harmonic generation from a nonlinear medium. The nature of a nonlinear Brewster angle is considered as a counterpart to the Brewster angle in the linear optical case. When the fundamental beam is incident upon a nonlinear medium of a specific crystallographic orientation, the reflected second-harmonic intensity $I_R(2\omega)$ vanishes at a particular angle of incidence called the nonlinear Brewster angle. The origin and physical interpretation of the nonlinear Brewster angle [1] can be understood in terms of classical dipole radiation. At the nonlinear Brewster angle, the fundamental beam will create a nonlinear polarization $\mathbf{P}^{\mathrm{NLS}}(2\omega)$ inside the medium in the direction of propagation of the reflected second-harmonic wave. According to classical dipole radiation theory, there is no radiation in this direction. This nonradiative wave upon refraction back into the linear medium would otherwise give rise to the reflected second-harmonic wave in the direction of $\mathbf{K}^R$. The reflected second-harmonic intensity $I_R(2\omega)$ vanishes

at the nonlinear Brewster angle when the nonlinear polarization source $\mathbf{P}^{\mathrm{NLS}}(2\omega)$ lies in the plane of incidence. Since the reflected second-harmonic intensity $I_R(2\omega)$ depends on the components of $\mathbf{P}^{\mathrm{NLS}}(2\omega)$ in the plane of incidence, therefore, measurement of the nonlinear Brewster angle, at which $I_R(2\omega)=0$, will directly yield the ratio of the components of $\mathbf{P}^{\mathrm{NLS}}(2\omega)$ in the plane of incidence, which could be helpful in determining the relative signs of various components of the $\chi^{(2)}$ tensor [19]. Hence measurement of the nonlinear Brewster angle could be applicable as a "null" method, which is similar to the work of Heinz, Tom, and Shen [22] for the precise measurement of the nonlinear optical susceptibility tensors.

It is interesting to point out that if the orientation of the KDP crystal as indicated in Fig. 6 is employed for studying the reflected second-harmonic intensity $I_R(2\omega)$ for the range $20°\leq\theta_i\leq 50°$, one can obtain a dip of $I_R(2\omega)$ at $\theta_i^{\mathrm{NB}}=42.83°$, which corresponds to the nonlinear Brewster angle of KDP that was observed experimentally [6] as shown in Fig. 8. Furthermore, by using the same crystallographic cut as indicated in Fig. 6 for ADP, the nonlinear Brewster angle of an ADP crystal has been theoretically predicted to be $\theta_i^{\mathrm{NB}}=43.32°$ [18].

It is worthwhile to point out that the prediction of a nonlinear Brewster angle in this work by using BP theory [1] is in good agreement with the prediction made by Dick *et al.* [19]. According to their paper, the reflected second-harmonic intensity generated from the nonlinear polarization $\mathbf{P}^{\mathrm{NLS}}(2\omega)$ in the plane of incidence is $I_P^R(2\omega)$. $I_P^R(2\omega)$ contains some vital terms in $F_{R,\parallel}^{\mathrm{NL}}$ of BP theory as given in Eq. (6). From Dick *et al.* [19], $I_P^R(2\omega)$ can be written as

$$I_P^R(2\omega)=\mathrm{const}\times|\cos\theta_T P_\xi^{\mathrm{NLS}}-\sin\theta_T P_\zeta^{\mathrm{NLS}}|^2\ , \tag{14}$$

where, according to Fig. 2, $P_\xi^{\mathrm{NLS}}$ is the component of $\mathbf{P}_\parallel^{\mathrm{NLS}}$ in the direction parallel to the surface of the nonlinear medium, $P_\zeta^{\mathrm{NLS}}$ is the component of $P_\parallel^{\mathrm{NLS}}$ in the direction normal to the surface of the nonlinear medium, and $P_\parallel^{\mathrm{NLS}}$ is the nonlinear polarization lying in the plane of incidence.

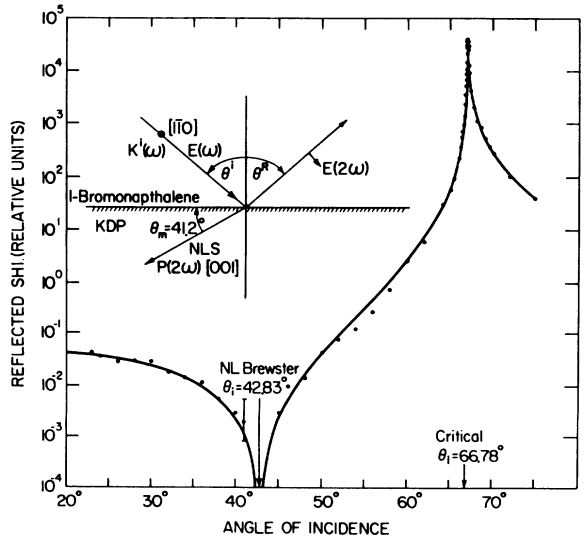


FIG. 8. Reflected second-harmonic intensity from KDP. The nonlinear Brewster angle of KDP crystal is first demonstrated at $\theta_i^{\mathrm{NB}}=42.83°$ [6].

The relationship of $P_\xi^{\mathrm{NLS}}$ and $P_\zeta^{\mathrm{NLS}}$ with $\mathbf{P}_\parallel^{\mathrm{NLS}}$ according to Fig. 2 can be written as

$$P_\xi^{\mathrm{NLS}}=P_\parallel^{\mathrm{NLS}}\sin(\alpha+\theta_S)\ ,\quad P_\zeta^{\mathrm{NLS}}=P_\parallel^{\mathrm{NLS}}\cos(\alpha+\theta_S)\ . \tag{15}$$

By substituting Eq. (15) into (14), the expression for $I_P^R(2\omega)$ is reduced to

$$I_P^R(2\omega)=\mathrm{const}\times|P_\parallel^{\mathrm{NLS}}\sin(\alpha+\theta_S+\theta_T)|^2\ , \tag{16}$$

where $\theta_S$, $\theta_T$, $\theta_R$, $\alpha$, and $P_\parallel^{\mathrm{NLS}}$ are defined in the same manner as in BP theory [1] as indicated in Fig. 2. Therefore Eq. (16), derived from the work of Dick *et al.* contains the same vital term $\sin(\alpha+\theta_S+\theta_T)$ in the expression for $F_{R,\parallel}^{\mathrm{NL}}$ in Eq. (16). The condition for the nonlinear Brewster angle given by [1,6,18,19] is

$$F_{R,\parallel}^{\mathrm{NL}}=0\ ,\quad \text{or } I_P^R(2\omega)=0\ ,$$

which leads to

$$\sin(\alpha+\theta_S+\theta_T)=0\ ,\quad \text{or } \alpha+\theta_S+\theta_T=0,\pi\ . \tag{17}$$

Therefore the ratio $P_\zeta^{\mathrm{NLS}}/P_\xi^{\mathrm{NLS}}$ can be obtained from Eq. (14). For the case of KDP having a crystallographic cut as indicated in Fig. 6 and the nonlinear Brewster angle experimentally observed [6], one can consider the crystal orientation as indicated in Fig. 9 with the polarization of the fundamental beam in the [1$\bar{1}$0] direction perpendicular to the plane of incidence. In this particular situation the crystallographic axes system $(X,Y,Z)$ and the surface axes system $(\xi,\eta,\zeta)$ are related through

$$\begin{bmatrix}\xi\\ \eta\\ \zeta\end{bmatrix}=\frac{1}{\sqrt{2}}\begin{bmatrix}\sin\varphi & \sin\varphi & -\sqrt{2}\cos\varphi\\ -1 & 1 & 0\\ \cos\varphi & \cos\varphi & \sqrt{2}\sin\varphi\end{bmatrix}\begin{bmatrix}X\\ Y\\ Z\end{bmatrix}\ . \tag{18}$$

Therefore, the nonlinear polarization components in the surface axes $P_\xi$ and $P_\zeta$ are related to $P_X$, $P_Y$, and $P_Z$ through

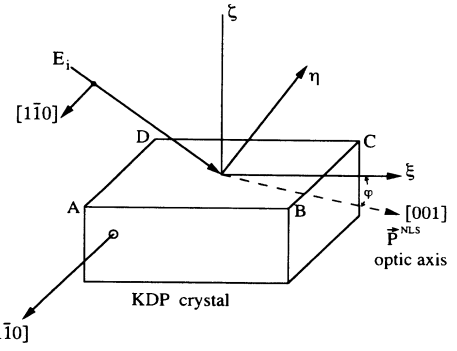


FIG. 9 Geometry indicating the crystallographic axes $(X,Y,Z)$ and the surface axes $(\xi,\eta,\zeta)$.

$$P_\xi = \frac{1}{\sqrt{2}}(P_X + P_Y)\sin\varphi - P_Z\cos\varphi \ , \tag{19}$$

$$P_\zeta = \frac{1}{\sqrt{2}}(P_X + P_Y)\cos\varphi + P_Z\sin\varphi \ . \tag{20}$$

Since the polarization of the fundamental beam is in the $[1\bar{1}0]$ direction, the nonlinear polarization $\mathbf{P}^{\mathrm{NLS}}(2\omega)$ is

$$P_Z(2\omega) = 2\chi_{36}E_X E_Y \quad \text{and} \quad P_X = P_Y = 0 \ .$$

Therefore, from Eqs. (19) and (20) the ratio of $P_\xi/P_\zeta$ is given by

$$P_\zeta/P_\xi = \tan\phi \ . \tag{21}$$

At the nonlinear Brewster angle, where $I_P^R(2\omega)=0$, the ratio of $P_\zeta^{\mathrm{NL}}/P_\xi^{\mathrm{NL}}$ can be obtained from Eq. (14) as

$$P_\zeta^{\mathrm{NL}}/P_\xi^{\mathrm{NL}} = \cot\theta_T \ . \tag{22}$$

For the KDP crystal used in this work, as indicated in Fig. 6, the nonlinear Brewster angle occurred at $\theta_i = 42.83°$ which has a corresponding $\theta_T$. Via the generalized Snell's law in Eq. (1), one obtains $\theta_T = 48.8°$. Therefore the angle

$$(\theta_T + \varphi) = (48.8° + 41.2°) = 90° \ .$$

Thus from Eq. (22) one obtains

$$P_\zeta^{\mathrm{NLS}}/P_\xi^{\mathrm{NLS}} = \cot\theta_T = \tan\varphi \ ,$$

leading to the ratio $P_\zeta^{\mathrm{NLS}}/P_\xi^{\mathrm{NLS}} = 0.8574$.

## V. CONCLUSION

In conclusion, second-harmonic generation was experimentally observed under the conditions of non-phase-matching and phase matching at total reflection. The experimental results verify the Bloembergen and Pershan theory and theory of Dick *et al.* Furthermore, demonstration of utilization of the nonlinear Brewster angle predicted by the BP theory may be applicable as a null method for the precise measurement of the relative magnitudes of nonlinear optical susceptibility components of materials.


[1] N. Bloembergen and P. Pershan, Phys. Rev. **128**, 606 (1962).
[2] J. Ducuing and N. Bloembergen, Phys. Rev. Lett. **10**, 474 (1963).
[3] N. Bloembergen, H. J. Simon, and C. H. Lee, Phys. Rev. **181**, 1261 (1969).
[4] P. P. Bey, J. F. Giuliani, and H. Rabin, Phys. Rev. **184**, 849 (1969).
[5] H. S. T. Shih and N. Bloembergen, Phys. Rev. A **3**, 412 (1971).
[6] C. H. Lee and V. Bhanthumnavin, Opt. Commun. **18**, 326 (1976).
[7] V. Bhanthumnavin and C. H. Lee, Microwave Opt. Technol. Lett. **3**, 279 (1990).
[8] P. W. Smith, W. J. Tomlinson, P. J. Maloney, and A. E. Kaplan, Opt. Lett. **7**, 57 (1982).
[9] A. E. Kaplan, Zh. Eksp. Teor. Fiz. **72**, 1710 (1977) [Sov. Phys. JETP **45**, 896 (1977)].
[10] D. L. Butler, G. L. Burdge, C. H. Lee, and H. J. Simon, Opt. Lett. **17**, 1125 (1992).
[11] H. J. Simon and C. H. Lee, Opt. Lett. **13**,. 440 (1988).
[12] C. S. Tsai, B. Kim, and F. R. El-Akkari, IEEE J. Quantum Electron. **14**, 513 (1978).
[13] S. K. Shum, Appl. Opt. **17**, 3679 (1978).
[14] M. R. Meadows, M. A. Handschy, and N. A. Clark, Appl. Phys. Lett. **54**, 1394 (1989).
[15] T. F. Heins, F. J. Himpsel, E. Palange, and E. Burstein, Phys. Rev. Lett. **63**, 644 (1989).
[16] M. S. Yeganeh, J. Qi, A. G. Yodh, and M. C. Tamargo, Phys. Rev. Lett. **68**, 3761 (1992).
[17] N. Bloembergen and C. H. Lee, Phys. Rev. **19**, 835 (1967).
[18] V. Bhanthumnavin and N. Ampole, Microwave Opt. Technol. Lett. **3**, 239 (1990).
[19] B. Dick, A. Gierulski, G. Marowski, and G. A. Reider, Appl. Phys B **38**, 107 (1985).
[20] G. D. Boyd, A. Askin, J .M. Dziedzic, and D. A. Kleinmann, Phys. Rev. **137**, A1305 (1965).
[21] P. D. Maker, R. W. Terhune, M. Nisenoff, and C. M. Savage, Phys. Rev. Lett. **8**, 21 (1962).
[22] T. F. Heinz, H. W. K. Tom, and Y. R. Shen, Phys. Rev. A **28**, 1883 (1983).